J|A|C|S ARTICLES

Published on Web 11/24/2009

# Ferromagnetic Nanoscale Electron Correlation Promoted by Organic Spin-Dependent Delocalization

Martin L. Kirk,*,† David A. Shultz,*,‡ Robert D. Schmidt,‡ Diana Habel-Rodriguez,† Hyoyoung Lee,*,§ and Junghyun Lee§

*Department of Chemistry and Chemical Biology, The University of New Mexico, MSC03 2060, 1 University of New Mexico, Albuquerque, New Mexico 87131-0001, Department of Chemistry, North Carolina State University, Raleigh, North Carolina 27695-8204, and NCRI Center for Smart Molecular Memory, Department of Chemistry, Sungkyunkwan University, Suwon 440-746, Republic of Korea*

Received June 8, 2009; E-mail: mkirk@unm.edu; David_Shultz@ncsu.edu; hyoyoung@skku.edu

***Abstract:*** We describe the electronic structure and the origin of ferromagnetic exchange coupling in two new metal complexes, NN-SQ-$Co^{III}(py)_2$Cat-NN (**1**) and NN-Ph-SQ-$Co^{III}(py)_2$Cat-Ph-NN (**2**) (NN = nitronylnitroxide radical, Ph = 1,4-phenylene, SQ = $S = {}^1/_2$ semiquinone radical, Cat = $S = 0$ catecholate, and py = pyridine). Near-IR electronic absorption spectroscopy for **1** and **2** reveals a low-energy optical band that has been assigned as a $\Psi_u \rightarrow \Psi_g$ transition involving bonding and antibonding linear combinations of delocalized dioxolene (SQ/Cat) valence frontier molecular orbitals. The ferromagnetic exchange interaction in **1** is so strong that only the high-spin quartet state ($S_T = {}^3/_2$) is thermally populated at temperatures up to 300 K. The temperature-dependent magnetic susceptibility data for **2** reveals that an excited state spin doublet ($S_T = {}^1/_2$) is populated at higher temperatures, indicating that the phenylene spacer modulates the magnitude of the magnetic exchange. The valence delocalization within the dioxolene dyad of **2** results in ferromagnetic alignment of two localized NN radicals separated by over 22 Å. The ferromagnetic exchange in **1** and **2** results from a spin-dependent delocalization (double exchange type) process and the origin of this strong electron correlation has been understood in terms of a valence bond configuration interaction (VBCI) model. We show that ferromagnetic coupling promoted by organic mixed-valency provides keen insight into the ability of single molecules to communicate spin information over nanoscale distances. Furthermore, the strong interaction between the itinerant dioxolene electron and localized NN electron spins impacts our ability to understand the exchange interaction between delocalized electrons and pinned magnetic impurities in technologically important dilute magnetic semiconductor materials. The long correlation length (22 Å) of the itinerant electron that mediates this coupling indicates that high-spin $\pi$-delocalized organic molecules could find applications as nanoscale spin-polarized electron injectors and molecular wires.

## Introduction

The exchange interaction between localized magnetic moments via delocalized conduction band electrons can lead to long-range magnetic order and ferromagnetic spin alignment in solid-state materials.[1−4] This delocalized electron-, or carrier-, mediated ferromagnetism also figures prominently in spintronic materials including dilute magnetic semiconductors (DMS). There have been considerable theoretical and experimental studies on DMS materials with the goal of understanding the nature of the ferromagnetic exchange interactions between doped magnetic impurity ions mediated by itinerant electron(s).[5−7] The mechanism of nanoscale electron correlation leading to ferromagnetic exchange between a delocalized electron and localized magnetic moments is complex and not completely understood. Notably, long-range ferromagnetic exchange between localized spins mediated by delocalized electrons has not been observed in molecular systems. Here we show that long-range electron correlation of localized radical spins, leading to ferromagnetic spin alignment, can be promoted by organic mixed-valency and spin-dependent electron delocalization. A high-spin $S_T = {}^3/_2$ ground state is found for NN-SQ-$Co^{III}(py)_2$Cat-NN (**1**) (py = pyridine), which possesses mixed-valent catecholate (Cat) and radical semiquinone (SQ) ligands elaborated with localized nitronylnitroxide (NN) radicals. The ferromagnetic exchange is so strong in this complex that there exists no evidence of

† The University of New Mexico.
‡ North Carolina State University.
§ Sungkyunkwan University.

(1) Lathiotakis, N. N.; Andriotis, A. N.; Menon, M. *Phys. Rev. B* **2008**, *78*, 193311.
(2) Zhu, Y.; Cao, J. X.; Yang, Z. Q.; Wu, R. Q. *Phys. Rev. B* **2009**, *79*, 085206.
(3) Ozgur, U.; Alivov, Y.; Liu, C.; Teke, A.; Reshchikov, M. A.; Dogan, S.; Avrutin, V.; Cho, S. J.; Morkoc, H. *J. Appl. Phys.* **2005**, *98*, 041301.
(4) Liu, E. Z.; He, Y.; Jiang, J. Z. *Appl. Phys. Lett.* **2008**, *93*, 132506.
(5) Kittilstved, K. R.; Gamelin, D. R. *J. Appl. Phys.* **2006**, *99*, 08M112.
(6) Chambers, S. A.; Droubay, T. C.; Wang, C. M.; Rosso, K. M.; Heald, S. M.; Schwartz, D. A.; Kittilstved, K. R.; Gamelin, D. R. *Mater. Today* **2006**, *9*, 28–35.
(7) Kittilstved, K. R.; Liu, W. K.; Gamelin, D. R. *Nat. Mater.* **2006**, *5*, 291–297.

 **10.1021/ja904648r** 

low-spin $S_T = {}^1/_2$ states being populated at room temperature. In addition, electron delocalization of the itinerant electron within the mixed-valent SQ/Cat dyad in NN-Ph-SQ-$Co^{III}(py)_2$Cat-Ph-NN (**2**) (Ph = 1,4-phenylene) results in a remarkable ferromagnetic alignment of *localized* NN radical spins separated by distances greater than 22 Å. These results clearly indicate that very long-range electron correlation can result in the transfer of spin information over nanoscale distances in magnetically dilute metallo−organic hybrid and related systems. Importantly, the itinerant electron in **1** and **2** couples with the localized NN moments via an excited-state donor−acceptor charge transfer configuration. That this occurs in a molecular system is of extreme interest since similar charge transfer mechanisms have been used to explain high $T_c$ ferromagnetism in DMSs.[6,7]

## Experimental Section

**General Considerations.** Elemental analyses (C, H, and N) were performed by Atlantic Microlab, Inc., Norcross GA. Infrared spectra were collected on a Perkin-Elmer Spectrum RX-1 FT-IR spectrometer for samples cast as a film from $CH_2Cl_2$ on a NaCl plate. X-band EPR spectra were recorded on an IBM-Brüker E200SRC continuous-wave spectrometer in fluid solution. Samples were dissolved in $CH_2Cl_2$ solution and spectra collected in quartz sample tubes. Fluid solution EPR spectra were simulated using WinSim to obtain accurate hyperfine coupling constants ($a_N$).[8] Toluene and $CH_2Cl_2$ were collected from an alumina column solvent purification system.[9] Q-Ph-NN and Cat-NN were prepared as described previously.[10,11] Lead dioxide and pyridine were purchased from Sigma Aldrich and used as received without further purification. Dicobalt octacarbonyl was purchased from Strem Chemicals and used as received without further purification.

**Preparation of Quinone-Nitronylnitroxide (Q-NN).** A 100 mL round-bottom flask containing Cat-NN (102 mg, 0.32 mmol) and 75 mL of $CH_2Cl_2$ is stirred at room temperature under nitrogen. An excess of $PbO_2$ is added (∼500 mg, 2.09 mmol) as a black solid, changing from a dark-blue to a dark-green solution. The mixture is stirred under nitrogen for 3 h to ensure completion. Excess $PbO_2$ is removed via filtration, and the solution evaporated to afford a green residue that was found to be unstable to atmosphere and degraded over time. The product was therefore carried through to the next step without purification. IR (film from $CH_2Cl_2$) $\nu$ in $cm^{-1}$: 2961, 2940, 2873, 1775, 1736, 1659, 1615, 1553, 1454, 1415, 1372, 1304, 1272, 1241, 1222, 1166, 1142, 1093, 977, 900, 876, 796, 734, 693, 652. EPR: fluid solution ∼0.2 mM in $CH_2Cl_2$, $a_N$ = 7.31 G.

**Preparation of $Co^{III}(py)_2$(Cat-NN)(SQ-NN) (1).** A 100 mL Schlenk flask containing Q-NN (101 mg, 0.32 mmol) and 40 mL of a 1:1 $CH_2Cl_2$/toluene solution is stirred at room temperature under nitrogen atmosphere. A solution of dicobalt octacarbonyl (27 mg, 0.08 mmol) in 15 mL of 1:1 $CH_2Cl_2$/toluene is added via cannulation followed by pyridine (0.03 mL, 0.32 mmol) added neat via syringe. The dark blue-green solution is heated to ∼35 °C, shielded from light, and left to stir for 6 h. Concentration under reduced pressure precipitates a dark blue solid (60 mg, 44%). IR (film from $CH_2Cl_2$) $\nu$ in $cm^{-1}$: 6091, 3573, 2951, 2865, 1769, 1660, 1598, 1575, 1447, 1429, 1396, 1373, 1281, 1212, 1143, 1000, 871, 831, 765, 730, 693. Analysis for $C_{44}H_{56}CoN_6O_8 \cdot C_6H_{12} \cdot 2CH_2Cl_2$: Calc C, 56.27; H, 6.54; N, 7.57. Found C, 56.03; H, 6.47; N, 7.67.

**Preparation of $Co^{III}(py)_2$(Cat-Ph-NN)(SQ-Ph-NN) (2).** A 100 mL Schlenk flask containing Q-Ph-NN (96 mg, 0.24 mmol) and 35 mL of a 1:1 $CH_2Cl_2$/toluene solution is stirred at room temperature under nitrogen atmosphere. A solution of dicobalt octacarbonyl (21 mg, 0.06 mmol) in 10 mL of 1:1 $CH_2Cl_2$/toluene is added via cannulation followed by pyridine (0.02 mL, 0.24 mmol) added neat via syringe. The dark blue-green solution is heated to ∼35 °C, shielded from light, and left to stir for 5 h. Concentration under reduced pressure precipitates a dark-blue solid (137 mg, 56%). IR (film from $CH_2Cl_2$) $\nu$ in $cm^{-1}$: 5941, 3563, 2941, 2588, 1597, 1476, 1450, 1417, 1384, 1362, 1274, 1211, 1132, 1073, 1006, 973, 926, 872, 830, 763, 734, 696, 637. Analysis for $C_{56}H_{64}CoN_6O_8 \cdot C_6H_{12} \cdot CH_2Cl_2$: Calc C, 64.28; H, 6.68; N, 7.14. Found C, 64.34; H, 6.47; N, 6.89.

**Magnetism.** Magnetic susceptibilities were measured on a Quantum Design MPMS-XL7 SQUID magnetometer using an applied field of 0.7 T for Curie plots. Microcrystalline samples were prepared by two methods: (1) samples were loaded into gel cap/straw sample holders and mounted to the sample rod with Kapton tape; (2) samples were loaded into a Delrin sample holder and screwed into the sample rod. Data from the gelcap samples were corrected for the sample container and molecular diamagnetism using Pascal's constants as a first approximation. The data were further corrected for inaccuracies in the diamagnetic correction by incorporation of a straight line into the overall fit expression, the slope of which represents the residual diamagnetic correction. The data for the Delrin samples were corrected for molecular diamagnetism through Pascal's constants and for the inherent diamagnetism of the sample holder by a background scan subtraction.

**NIR Electronic Absorption Spectroscopy.** Spectra were collected on a Perkin-Elmer Spectrum RX-1 FT-IR spectrometer for samples cast as evaporated thin-films from $CH_2Cl_2$ on a NaCl plate. Solutions of **1** and **2** were prepared using four different solvents (1,2-$Cl_2C_2H_4$, $CH_2Cl_2$, $CCl_4$ and $CS_2$, see Supporting Information) and loaded into a KBr cavity cell for sample collection. Pure solvent spectra were collected for background correction.

**X-ray Crystallography.** X-ray crystallography for complex **1** was conducted at the X-ray Structural Facility at North Carolina State University. Data collection and refinement for complex **2** were conducted at the X-ray facility at the University of Michigan. A complete description of the data collected is reported in the Supporting Information.

**Electronic Structure Calculations.** Spin-unrestricted gas-phase geometry optimizations for compounds **1** and **2** were performed at the density functional level of theory using the Gaussian 03W software package.[12] All calculations employed the B3LYP hybrid functional. A 6-31G* basis set, including polarization functions, was used for all atoms except Co, where a LANL2DZ basis set was employed. Input files were prepared using the molecule builder function in the Gaussview software package. Time-dependent density functional theory was used to calculate the first 60 electronic transitions.

## Results

**X-ray Crystallography.** Schematic structures of both **1** and **2** are depicted in Figure 1 along with ORTEP drawings of their X-ray structures (see Supporting Information for crystallographic details). Compound **1** exists as two crystallographically independent molecules in the unit cell. Important bond lengths for **1** and **2** are compared with those of *bona fide* SQ and Cat ligands in Table 1. The data in Table 1 show that both the dioxolene (dioxolene = SQ/Cat) C−O and C−C bond lengths for **1** and **2** are roughly the average of those observed in $Tp^{Cum,Me}Co^{II}$(3,5-

(8) Duling, D. *EPR calculations for MS-Windows NT 95*, Version 0.96 ed.; EPR Software Tools, National Institute of Environmental Health Sciences, National Institutes of Health: Triangle Park, NC, 1996.
(9) Pangborn, A. B.; Giardello, M. A.; Grubbs, R. H.; Rosen, R. K.; Timmers, F. J. *Organometallics* **1996**, *15*, 1518.
(10) Shultz, D. A.; Bodnar, S. H.; Vostrikova, K. E.; Kampf, J. W. *Inorg. Chem.* **2000**, *39*, 6091–6093.
(11) Shultz, D. A.; Vostrikova, K. E.; Bodnar, S. H.; Koo, H. J.; Whangbo, M. H.; Kirk, M. L.; Depperman, E. C.; Kampf, J. W. *J. Am. Chem. Soc.* **2003**, *125*, 1607–1617.
(12) Frisch, M. J.; et al. *Gaussian 03*; Gaussian, Inc.: Wallingford, CT, 2004. Frisch, M. J.; et al. *Gaussian 03*; Gaussian, Inc.: Pittsburgh, PA, 2003.

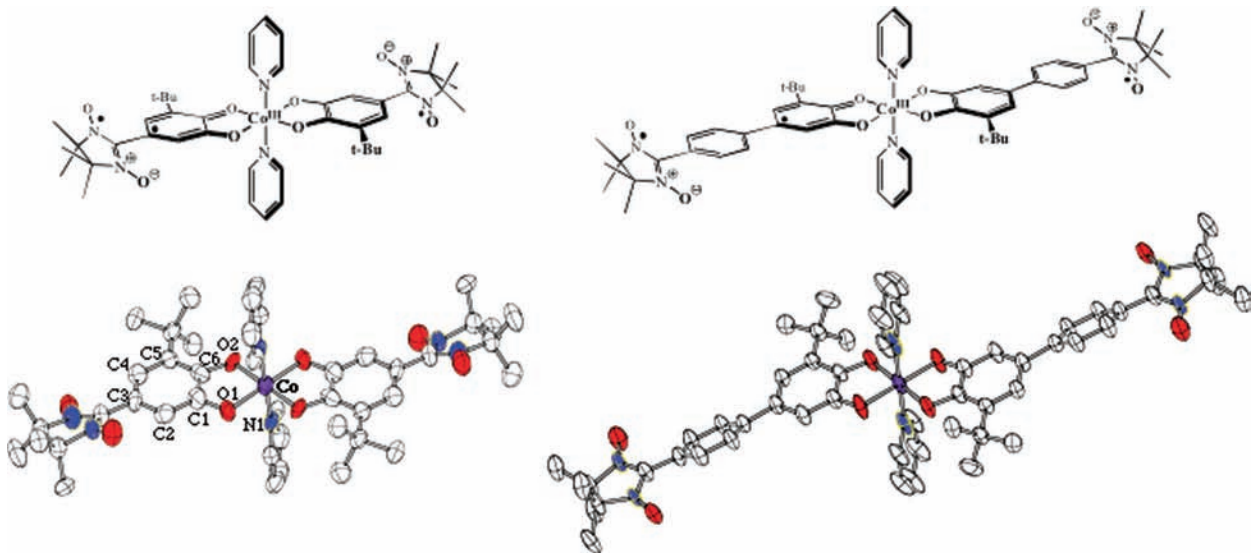


***Figure 1.*** Structures of NN-SQ-$Co^{III}(py)_2$Cat-NN (**1**) and NN-Ph-SQ-$Co^{III}(py)_2$Cat-Ph-NN (**2**). (Top) Bond line drawings of **1** and **2**. (Bottom) ORTEPs of **1** and **2**. Hydrogen atoms and solvent molecules have been omitted for clarity.

***Table 1.*** Selected Bond Lengths (Å)

| | 1a | 1b | 2 | SQ[a] | Cat[b] | average |
|---|---|---|---|---|---|---|
| Co−O1 | 1.885 | 1.888 | 1.873 | − | | − |
| Co−O2 | 1.889 | 1.899 | 1.86 | − | | − |
| Co−N1 | 1.951 | 1.945 | 1.93 | − | − | − |
| O1−C1 | 1.313 | 1.38 | 1.324 | 1.301 | 1.349 | 1.325 |
| O2−C6 | 1.365 | 1.335 | 1.321 | 1.271 | 1.348 | 1.310 |
| C1−C2 | 1.41 | 1.426 | 1.384 | 1.443 | 1.368 | 1.406 |
| C2−C3 | 1.363 | 1.423 | 1.379 | 1.377 | 1.386 | 1.382 |
| C3−C4 | 1.443 | 1.405 | 1.404 | 1.441 | 1.391 | 1.416 |
| C4−C5 | 1.383 | 1.388 | 1.368 | 1.359 | 1.393 | 1.376 |
| C5−C6 | 1.437 | 1.46 | 1.418 | 1.396 | 1.391 | 1.394 |
| C6−C1 | 1.449 | 1.384 | 1.416 | 1.461 | 1.402 | 1.432 |

[a] SQ = $(Tp^{Cum,Me})Co^{II}$(3,5-DBSQ).[13] [b] Cat = $Mn^{IV}(py)_2$(3,5-DBCat)$_2$.[14] [c] Average = (SQ + Cat)/2.

DB**SQ**)[13] and $Mn^{IV}(py)_2$(3,5-DB**Cat**)$_2$,[14] suggesting Class III[15] delocalization in the SQ/Cat dyad. However, crystallographically imposed inversion centers coincident with the molecular $C_2$ axes are found in the structures of both **1** and **2**, and give the impression that the SQ/Cat dyads are completely delocalized Class III species.[15] Therefore, X-ray crystallography cannot distinguish between averaged bond lengths due to positional disorder and averaged bond lengths due to electron (SQ/Cat) delocalization. A close inspection of the bond lengths within the dioxolene rings (Table 1) and comparison to typical values for SQ and Cat merely confirm that the complex exists in the $[Co^{III}(diox)_2]^0$ oxidation state.

**Electronic Absorption Spectroscopy.** We obtained IR−NIR electronic absorption spectra of **2** in four solvents and as an evaporated thin film cast from $CH_2Cl_2$ (see Supporting Information for additional spectra of **1** and **2**). The $CS_2$ solution and thin film spectra for **2** are presented in Figure 2. These spectra display a low-energy band maximum in the 3300−3600 $cm^{-1}$ range with absorption intensity that extends out to ∼6000 $cm^{-1}$. Although instrument limitations preclude the collection of higher-quality spectra, the absorption envelope appears to include some vibronic structure. Similar, albeit less structured, low-energy electronic absorption bands have been observed in other SQ-$Co^{III}$(diimine)Cat complexes,[16] including the related NN-Ph-SQ-$Co^{III}$(bpy)Cat-Ph-NN,[17] that display effective $C_2$ symmetry within the $Co(diox)_2$ core and an ∼66° dihedral angle between the SQ and Cat planes. In all of these cases, the IR−NIR absorption band has been assigned as a classic Cat → SQ intervalence charge transfer (IVCT) band, and the complexes have been described as being in the Robin and Day Class II limit since the degree of electron delocalization in solution was not able to be directly determined.[18−20]

**Magnetic Susceptibility Measurements.** The nature of the ground spin state, radical−radical exchange couplings, and the ground-state electronic structure has been probed by variable-temperature magnetic susceptibility studies. The variable-temperature magnetic susceptibility data for **1** and **2** were collected from 2−300 K in an applied magnetic field of 0.7 T, and the data are plotted as the product of the paramagnetic susceptibility and the temperature ($\chi_{para}T$) in Figure 3. It is interesting to note that the $\chi_{para}T$ product for **1** is temperature independent above 50 K and displays Curie−Weiss behavior, consistent with an $S_T = {}^3/_2$ paramagnet and indicating that only a single spin state is populated at room temperature (Figure 3A). In contrast to the behavior of **1**, the $\chi_{para}T$ data for **2** (Figure 3B) decreases for temperatures above ∼50 K, and this is indicative of lower multiplicity spin states being populated at these elevated temperatures. The maximum value of $\chi_{para}T$ for both **1** and **2** is very close to 1.88 emu·K·$mol^{-1}$, the theoretical $\chi_{para}T$ value for an $S_T = {}^3/_2$ ground state. An $S_T = {}^3/_2$ ground state can only result from dominant pairwise ferromagnetic exchange coupling between SQ and the two NN spin centers in these molecules. The $\chi_{para}T$ product is observed to decrease

(13) Ruf, M.; Noll, B. C.; Groner, M. D.; Yee, G. T.; Pierpont, C. G. *Inorg. Chem.* **1997**, *36*, 4860–4865.
(14) Lynch, M. W.; Hendrickson, D. N.; Fitzgerald, B. J.; Pierpont, C. G. *J. Am. Chem. Soc.* **1984**, *106*, 2041–2049.
(15) Robin, M. B.; Day, P. *Adv. Inorg. Radiochem.* **1967**, *10*, 247.
(16) Adams, D. M.; Noodleman, L.; Hendrickson, D. N. *Inorg. Chem.* **1997**, *36*, 3966–3984.
(17) Shultz, D. A.; Krishna Kumar, R.; Bin-Salamon, S.; Kirk, M. L. *Polyhedron* **2005**, *24*, 2876–2879.
(18) Ruiz, D.; Yoo, J.; Guzei, I. A.; Rheingold, A. L.; Hendrickson, D. N. *Chem. Commun.* **1998**, 2089–2090.
(19) Ruiz-Molina, D.; Zakharov, L. N.; Rheingold, A. L.; Hendrickson, D. N. *J. Phys. Chem. Solids* **2004**, *65*, 831–837.
(20) Evangelio, E.; Hendrickson, D. N.; Ruiz-Molina, D. *Inorg. Chim. Acta* **2008**, *361*, 3403–3409.

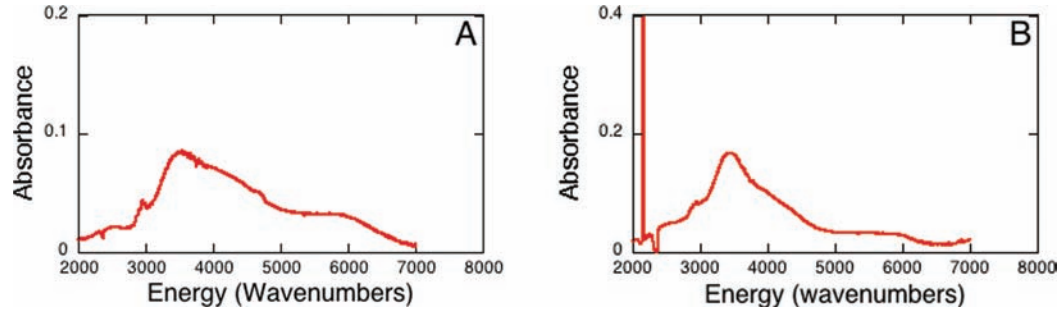


***Figure 2.*** Room temperature near-IR absorption spectra of NN-Ph-SQ-Co$^{III}$(py)$_2$Cat-Ph-NN (**2**). (A) Spectrum collected as a thin film cast from $CH_2Cl_2$. (B) Spectrum collected in $CS_2$.

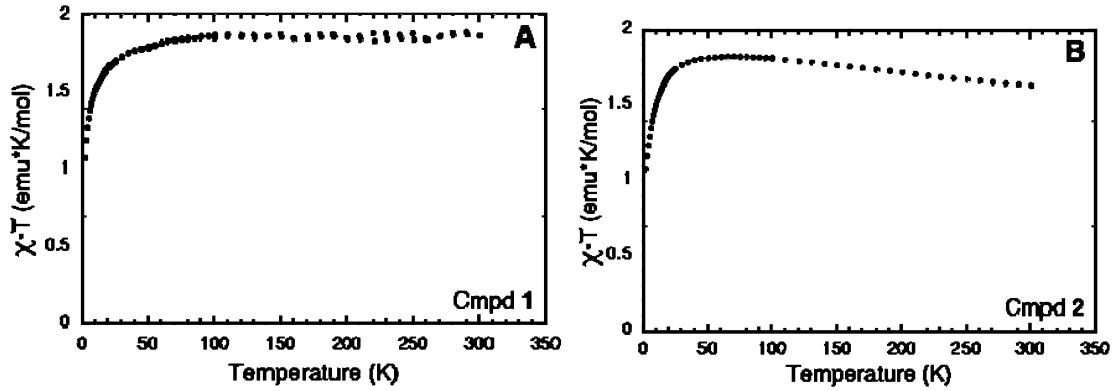


***Figure 3.*** (A) Paramagnetic susceptibility ($\chi_{para}$) of **1** plotted as $\chi_{para}T$ vs $T$. Only the $S_T = {}^3/_2$ state is populated at all temperatures measured for **1**. (B) Paramagnetic susceptibility ($\chi_{para}$) of **2** plotted as $\chi_{para}T$ vs $T$. All data were collected in an applied magnetic field of 0.7 T.

at temperatures below ~50 K for both **1** and **2**. This is a characteristic feature of these complexes and most likely results from intermolecular interactions that are treated using the Weiss correction. Zero-field splitting (ZFS) of an $S > {}^1/_2$ ground state could also result in a reduction of the $\chi_{para}T$ product at low temperatures. However, the spin−orbit coupling constants of the second row atoms that constitute the NN and SQ radicals are very small. This results in a reduced out-of-state spin−orbit coupling between the ground and excited states, and a negligibly small ZFS that will be dominated by dipolar terms.[11]

## Analysis

**Delocalization, the Nature of the Low-Energy Charge Transfer Band, and Interstate Vibronic Coupling.** Complexes **1** and **2** both possess *planar* Co(diox)$_2$ cores with an effective $C_{2h}$ symmetry. This is in marked contrast to NN-Ph-SQ-Co$^{III}$(bpy)Cat-Ph-NN, which possesses effective $C_2$ symmetry and a distinctly *nonplanar* Co(diox)$_2$ core with an ~66° dihedral angle between the dioxolene planes.[17] Due to the planarity of the Co(diox)$_2$ core in **1** and **2**, we hypothesized that the degree of electron delocalization should be notably larger than that observed in NN-Ph-SQ-Co$^{III}$(bpy)Cat-Ph-NN and other $C_2$ type Co$^{III}$(diimine)(Cat)(SQ) systems. Electronic structure calculations performed on the high spin ($S_T = {}^3/_2$) ground state indicate planar Co(diox)$_2$ cores and a complete delocalization of the positive spin density across the entire molecule in both **1** and **2** (Figure 4). This differs from the degree of delocalization determined for $C_2$-symmetric NN-Ph-SQ-Co$^{III}$(bpy)Cat-Ph-NN, which was estimated to be <15% from the ratio of the magnetic exchange coupling parameters, $J_{NN(B)\text{-}SQ(A)}/J_{NN(A)\text{-}SQ(A)}$ (*vide infra*, see Supporting Information), where A and B indicate NN and dioxolene sites on the left and right-hand side of the molecule, respectively. Taken together, these results indicate that the

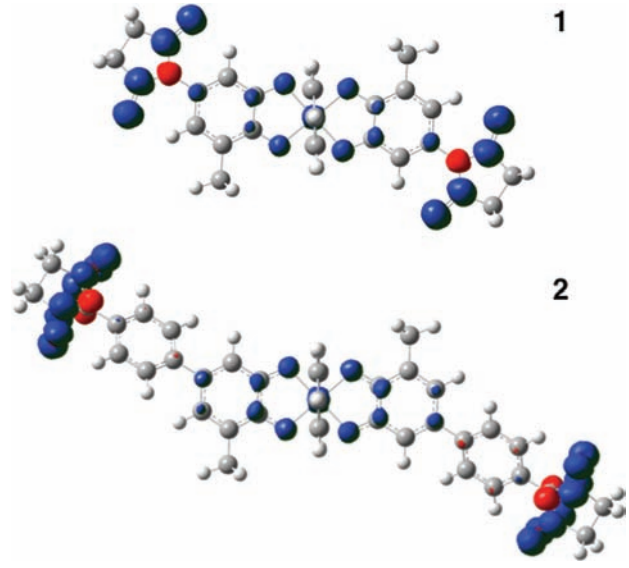


***Figure 4.*** Calculated spin densities for the $S = {}^3/_2$ ground states of **1** (top) and **2** (bottom). Regions of positive spin density are shown in blue and regions of negative spin density are shown in red. Note the symmetric delocalization of positive spin density across the entire molecule in both **1** and **2**.

planarity of the Co(diox)$_2$ core in both **1** and **2** may facilitate a considerably greater degree of electron delocalization compared to their $C_2$ analogues.

For Class III valence delocalized species, a spin- and dipole-allowed optical transition should be observed with an energy that is directly related to the magnitude of the electronic coupling matrix element, $H_{AB}$. In the intermediate Class II delocalization limit, this is described as a classical IVCT transition involving

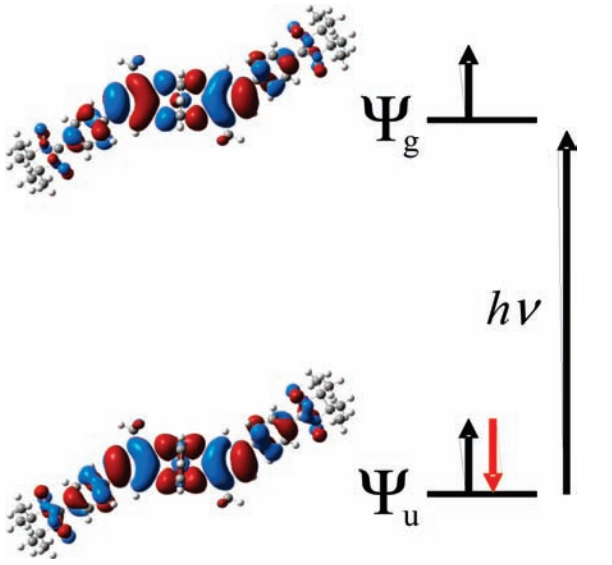


***Figure 5.*** Molecular orbitals principally involved in the NIR $\Psi_u \rightarrow \Psi_g$ transition for **2**. View is oriented down the py-Co-py axis.

a one electron promotion from an orbital, $\phi_B$, localized on Cat to an acceptor orbital, $\phi_A$, localized on SQ.[15,21] However, in the limit of complete Class III electron delocalization, this transition is a bonding to antibonding $\Psi_u \rightarrow \Psi_g$ transition, where $\Psi_{u,g} = 2^{-1/2}(\phi_A \pm \phi_B)$ (Figure 5).[15,22,23]

Time-dependent DFT (TDDFT) calculations performed on the delocalized ground states of **1** and **2** indicate an intense $\Psi_u \rightarrow \Psi_g$ transition at 3700 $cm^{-1}$, in very good agreement with the experimental 3500 $cm^{-1}$ absorption band maximum that we observe for both **1** and **2** (Figure 2; see Supporting Information for the spectrum of **1**). In the effective $C_{2h}$ symmetry of the *delocalized* $Co(diox)_2$ core present in **1** and **2**, the $\Psi_u^2\Psi_g^1$ configuration yields a state of $^4A_u$ symmetry (considering also the symmetries of the two half-filled NN-based orbitals), while the $\Psi_u^1\Psi_g^2$ first excited configuration yields an excited state of $^4B_g$ symmetry. Two energetically proximate states of the same multiplicity are subject to distortion through a vibration which transforms as the direct product of the two states. Thus, the $^4A_u$ ground state is susceptible to a distorting force, $F$, which results from vibronic coupling with the $^4B_g$ excited state (eq 1).

$$F = \left\langle {}^4A_u \left| \left(\frac{\partial V}{\partial Q}\right)_{Q^*} \right| {}^4B_g \right\rangle \qquad (1)$$

This will warp the ground-state potential energy surface and result in a double-well potential with a more localized (i.e., Class II) electronic structure description. The symmetry of the vibration that leads to this localization is determined from the direct product $\Gamma_{A_u} \otimes \Gamma_{B_g} = \Gamma_{(\partial V/\partial Q)_{Q^*}}$. As shown in Figure 6, the distorting mode which couples the $^4A_u$ and $^4B_g$ states transforms as $b_u$.

The $^4B_g$ excited state is expected to dominate vibronic coupling contributions to the $^4A_u$ ground state due to the very small energy gap (~0.5 eV) between these two states, and this results in an in-plane distortion of $b_u$ symmetry that can lead to electronic localization within the $Co(diox)_2$ cores of **1** and **2** (Figure 6). Thus, the stabilization leading to electron delocalization is in direct opposition to the stabilization gained by vibronic coupling leading to localization. Although the calculated spin density distributions and nature of the low-energy electronic transitions strongly suggest an electronic structure description of **1** and **2** that approaches the Class III limit, the apparent disorder in the crystal structures of **1** and **2** precludes us from determining whether a static $b_u$ distortion is responsible for Class II behavior or whether these molecules possess true inversion symmetry and are significantly more delocalized at the Class II/III or Class III limits. However, the quality of the structures is sufficient to determine that the $Co(diox)_2$ cores of **1** and **2** are indeed planar. The observed planarity in **1** and **2** is important, since higher energy MLCT and LMCT states can also vibronically couple with the $^4A_u$ ground state and lead to *nonplanar* distortions of the $Co(diox)_2$ cores.

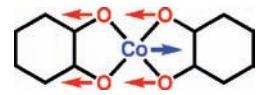


***Figure 6.*** Representation of the in-plane $b_u$ symmetry breaking mode that results from vibronic coupling between the delocalized $^4A_u$ ground state and the $^4B_g$ excited state. This distortion is responsible for electronic localization within the $Co(diox)_2$ cores of **1** and **2**.

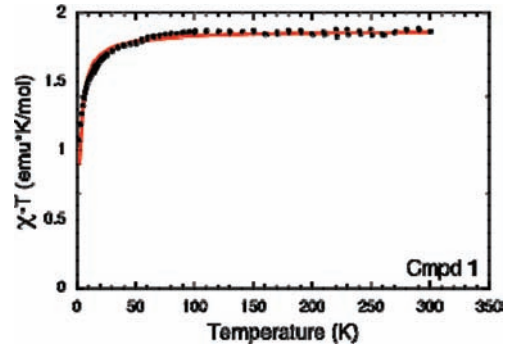


***Figure 7.*** Paramagnetic susceptibility ($\chi_{para}$) of **1** plotted as $\chi_{para}T$ vs $T$. The red line represents the best fit of the data to the Curie−Weiss model described in the text. The Weiss parameter, $\theta$, was determined to be −2 K and indicates weak intermolecular interactions in **1**.

**Magnetic Exchange Coupling.** In order to further explore the degree of electron delocalization in **1** and **2**, and to understand the electronic origin of their high-spin ($S_T = {}^3/_2$) ground states, we have probed the nature of the ground state electronic structure via variable-temperature magnetic susceptibility studies. The $\chi_{para}T$ product for **1** is temperature independent above 50 K, and the data have been fit to a Curie−Weiss model (eq 2) consistent with an $S = {}^3/_2$ paramagnet (Figure 7). Here $T$ is the temperature, $S$ is the total spin value ($S_T = S = {}^3/_2$), $N$ is Avogadro's number, $g$ is the isotropic $g$-value, $\beta$ is the Bohr magneton, and $k_B$ is Boltzmann's constant.

$$\chi_{para}T = \frac{Ng^2\beta^2T}{3k_B(T-\theta)}S(S+1);\ S = 3/2 \qquad (2)$$

The best fit of eq 2 to the data yields a negative Weiss parameter ($\theta = -2$ K), which indicates that weak intermolecular antiferromagnetic interactions are present and responsible for

(21) Hush, N. S. *Prog. Inorg. Chem.* **1967**, *8*, 391–444.
(22) Bersuker, I. B. *Electronic Structure and Properties of Transition Metal Compounds. Introduction to the Theory*; Wiley-Interscience: New York, 1996.
(23) Gamelin, D. R.; Bominaar, E. L.; Mathoniere, C.; Kirk, M. L.; Wieghardt, K.; Girerd, J.-J.; Solomon, E. A. *Inorg. Chem.* **1996**, *35*, 4323–4335.

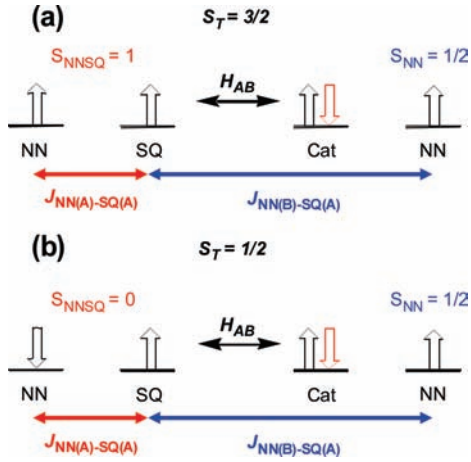


***Figure 8.*** Schematic description of electron delocalization ($H_{AB}$) and SQ/Cat pairwise HDvV magnetic exchange pathways in **2**. Note that in TM systems, the "single site" exchange interaction described by $J_A$ can be $>10^5$ cm$^{-1}$. This is 2−3 orders of magnitude greater than that found in **2**, leading to a strong resonance interaction between the $|S_T = {}^1/_2, S_{NNSQ} = 1, S_{NN} = {}^1/_2\rangle$ and "non-Hund" $|S_T = {}^1/_2, S_{NNSQ} = 0, S_{NN} = {}^1/_2\rangle$ configurations.

the downward turn in the data below ~50 K. In marked contrast to the $S = {}^3/_2$ paramagnetic nature of **1**, the $\chi_{para}T$ data for **2** decreases at temperatures above ~50 K, indicating the population of lower multiplicity spin states. We begin the analysis of **2** by treating the $\chi_{para}T$ data in the localized Class I/II limit, which derives from vibronic trapping due to a localizing $b_u$ distorting mode or a lack of resonance delocalization. The appropriate Heisenberg spin Hamiltonian for this situation is given in eq 3 for an unsymmetrically coupled system, which explicitly treats the NN(A)-SQ(A) exchange interaction ($J_{NN(A)-SQ(A)}$) on the left-hand side of **2** and the NN(B)-SQ(A) exchange interaction ($J_{NN(B)-SQ(A)}$) on the right-hand side of **2**.

$$\hat{H}_{HDvV} = -2J_{NN(A)-SQ(A)}(\hat{S}_{NN(A)}\cdot\hat{S}_{SQ(A)}) - 2J_{NN(B)-SQ(A)}(\hat{S}_{NN(B)}\cdot\hat{S}_{SQ(A)}) \quad (3)$$

Equation 3 describes the two magnetic exchange pathways present in **1** and **2** in the Class I/II limit, and these pathways are depicted in Figure 8. Operating with this Hamiltonian on the $|S_{NN(A)}, S_{SQ(A)}, S_{NN(B)}\rangle$ spin bases yields a spin quartet and two spin doublet states with the following energies, where $J_A = J_{NN(A)-SQ(A)}$ and $J_B = J_{NN(B)-SQ(A)}$.

$$E_Q = -\frac{J_A + J_B}{2}$$
$$E_{D_A,D_B} = \frac{J_A + J_B}{2} \pm \sqrt{J_A^2 + J_B^2 - J_AJ_B} \quad (4)$$

Inspection of the structure for **2** indicates that the shortest through-bond exchange coupling pathway between SQ(A) and NN(B) is over 11 bonds, and should be appreciably weaker than the NN(A)-SQ(A) exchange interaction, which is only over 5 bonds. From the distance dependence of $J$ (eq 5),[24,25] the anticipated ratio of 11-bond to 5-bond $J$-values can be calculated using distances from the X-ray crystal structures. A $\beta$-value of 0.5 is typical for a 1,4-phenylene bridge,[26] where the distances

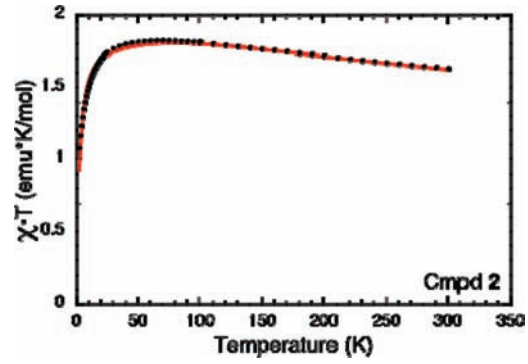


***Figure 9.*** Paramagnetic susceptibility ($\chi_{para}$) of **2** plotted as $\chi_{para}T$ vs $T$. The red line represents the best fit of the data to the HDvV model described in the text with $J_{NN(B)-SQ(A)} = J_{NN(A)-SQ(A)} = +234$ cm$^{-1}$.

between NN radicals obtained from the X-ray structures of **2** and $Tp^{CumMe}Zn(SQ\text{-}Ph\text{-}NN)$[11] yield $r \approx 16$ Å and $r_o \approx 7$ Å, respectively. This leads to a ratio of $J_{11\text{-bond}}/J_{5\text{-bond}} = 10^{-2}$.

$$J = J_o\, e^{-\beta(r-r_o)} \quad (5)$$

Thus, the exchange parameter over 11 bonds is expected to be 100-times weaker than the corresponding exchange over 5 bonds. To obtain experimental values of $J_{NN(A)-SQ(A)}$ (5 bonds) and $J_{NN(B)-SQ(A)}$ (11 bonds) the exchange energies that derive from eq 4 can be inserted into the field-independent van Vleck expression (eq 6), where the best fit of the equation to the $\chi_{para}T$ data for **2** is shown in Figure 9, with values summarized in Table 3.

$$\chi_{para}T = \frac{Ng^2\beta^2T}{3k_B(T-\theta)}\left[\frac{\sum_S S(S+1)(2S+1)\, e^{-E_s/k_BT}}{\sum_S S(S+1)\, e^{-E_s/k_BT}}\right] \quad (6)$$

Analysis of the magnetic data allows for the degree of spin-dependent delocalization in **1** and **2** to be probed through the ratio $J_{NN(B)-SQ(A)}/J_{NN(A)-SQ(A)}$. In the limit of complete SQ/Cat localization (i.e., Class I behavior in the Robin and Day scheme[15]), the localized SQ(A) spin would preclude any measurable exchange interaction between SQ(A) and NN(B) due to the extremely long 11-bond pathway, and the $J_{NN(B)-SQ(A)}/J_{NN(A)-SQ(A)}$ ratio would approach $10^{-2}$ (*vide supra*). However, full Class III behavior would yield an energetically stabilized $S = {}^3/_2$ ground state due to spin-dependent delocalization and a $J_{NN(B)-SQ(A)}/J_{NN(A)-SQ(A)}$ ratio of unity. Values of $J_{NN(B)-SQ(A)}/J_{NN(A)-SQ(A)}$ between 0 and 1 would define the Class II regime. We recall that the ferromagnetic exchange coupling in **1** is so strong that only the $S_T = {}^3/_2$ ground state is thermally populated at all temperatures measured (Figure 3A). Thus the $J_{NN(B)-SQ(A)}/J_{NN(A)-SQ(A)}$ ratio cannot be determined for compound **1**. However, for compound **2** the best fit of the susceptibility expression derived through the application of eqs 4 and 6 yields $J_{NN(B)-SQ(A)} = J_{NN(A)-SQ(A)} = +234$ cm$^{-1}$. The energy level spectrum for **2** is depicted in Figure 10. The fact that $J_{NN(B)-SQ(A)} = J_{NN(A)-SQ(A)}$ provides strong evidence for delocalization and an apparent Class II/III to Class III description for the mixed-valent Cat/SQ ligands in **2** and, by inference, compound **1** as well.

**Solvent Dependence of the IVCT/$\Psi_u \rightarrow \Psi_g$ NIR band.** With the magnetic data supporting strong delocalization in this system, we turn to a more classical approach to establishing mixed-valency and delocalization in the spectroscopic analysis of the

(24) Newton, M. D. *Chem. Rev.* **1991**, *91*, 767.
(25) Kanter, F. J. J. D.; Kaptein, R.; Vansanten, R. A. *Chem. Phys. Lett.* **1977**, *45*, 575–579.
(26) Welter, S.; Salluce, N.; Belser, P.; Groeneveld, M.; De Cola, L. *Coord. Chem. Rev.* **2005**, *249*, 1360–1371.

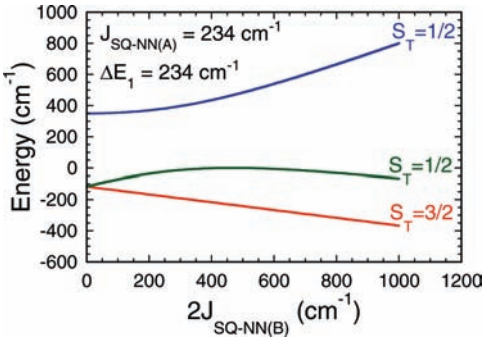


***Figure 10.*** Energy level spectrum from the HDvV Hamiltonian used in the analysis of the magnetic data for **2**. Note that extensive mixing occurs between the two $S_T = {}^1/_2$ doublet states.

***Table 2.*** Solvent Effect Summary for NIR Feature of **2**

| solvent | dielectric constant ($\varepsilon$) at 295 K[30] | $\nu_{max}$ ($cm^{-1}$) | $\Delta\nu_{1/2}$ ($cm^{-1}$)[a] | $\Delta\nu^2_{1/2}/\nu_{max}$ ($cm^{-1}$)[b] |
|---|---|---|---|---|
| 1,2-$Cl_2C_2H_4$ | 10.10 | 3604 | 1514 | 636 |
| $CH_2Cl_2$ | 8.93 | 3614 | 1514 | 634 |
| $CS_2$ | 2.63 | 3438 | 1046 | 318 |
| $CCl_4$ | 2.24 | 3390 | 1667 | 820 |

[a] Peak bandwidth at half-height calculated for maximum possible width of band 2, centered ~3500 $cm^{-1}$. [b] Hush prediction for Class II = 2312 $cm^{-1}$.[21]

NIR band to support this analysis. It is well established that systems in the Class II mixed-valent regime are very sensitive to solvent, and changing the dielectric constant of the solvent will shift the band maximum, often in excess of 1000 $cm^{-1}$.[27−29] There are also systems that are presented as Class III delocalized yet still demonstrate solvent dependence (~100−400 $cm^{-1}$).[29] For those systems described as borderline, Class II/III IVCT band shifts of 1000−2500 $cm^{-1}$ have been reported.[28,29] Electronic absorption spectra for **2** were collected in several different solvents (see also Supporting Information), to assess solvent dependence on band maxima and band shapes. The results are presented in Table 2, where the band maximum and bandwidth at half-height are taken as the maximum possible bandwidth for the primary asymmetric feature at ~3500 $cm^{-1}$.

The NIR band near 3500 $cm^{-1}$ is clearly solvent dependent, but the shift is only ~210 $cm^{-1}$, far less than that expected for a Class II mixed-valent system, and contrary to the behavior predicted by Marcus theory, where low dielectric solvents should shift the band to higher energy.[21] Also, the maximum possible ratio $\Delta\nu^2_{1/2}/\nu_{max}$ is ~25% of the Hush prediction of 2312 $cm^{-1}$.[21] The Hush prediction is most accurate in the Class II regime, and near the Class I/II border. Once delocalization approaches the Class II/III and Class III limits, the utility of the Hush relationships vanishes. Therefore, values of $\Delta\nu^2_{1/2}/\nu_{max}$ less than 2312 $cm^{-1}$ suggest delocalization either at the Class II/III limit, or deeper into the Class III regime. This presents a limitation of the spectroscopic analysis of delocalized and mixed-valent systems: the distinction between Class I and Class II is very clear—evidenced by the presence or absence of an IVCT band—whereas there is not always a clear distinction between Class II and Class III. Thus, the latter regimes exist as a continuum. Spectral features of band shape, solvent effects, and band asymmetry are presented as evidentiary for both Class II *and* Class III systems.[21] In the present case, the use of exchange coupling of pendant, localized NN radicals to report on the level of delocalization within the mixed-valent SQ/Cat dyad is perhaps superior to band shape analyses, as the coupling between the localized NN spins on opposite ends of the molecule can only be achieved in the limit of strong delocalization within the mixed-valent SQ/Cat dyad. Spectroscopic evidence combined with the modeling of variable-temperature magnetic susceptibility provides strong support for delocalization in **2** at the Class II/III border or perhaps deeper into the Class III regime.

**Spin-Dependent Delocalization.** The HDvV exchange analysis indicates a high level of delocalization in **1** and **2**, a result supported by the spectroscopic studies of the NIR band and computational results. In order to further elaborate on their mixed-valent nature and to correlate the ground state of **2** with the excited-state electronic structure, we have applied a more suitable spin-dependent delocalization (SDD) model[22,31−33] to this problem. A spin-dependent delocalization model is appropriate for analyzing the magnetic and spectroscopic properties of these systems since an itinerant electron is present in the mixed-valent dioxolene fragments of **1** and **2**. The spin-dependent delocalization Hamiltonian matrices for the $S_T = {}^3/_2$ and ${}^1/_2$ states are given in eq 7, where $J = J_{NN(A)\text{-}SQ(A)}$. This Hamiltonian yields a modified energy spectrum with twice the number of $S_T$ states generated by the HDvV Hamiltonian.[22,31,32,34−36]

$$\hat{H}_{S_T=3/2} = \begin{array}{c|cc} |S_T,S_A,S_B\rangle & \left|\frac{3}{2},1,\frac{1}{2}\right\rangle & \left|\frac{3}{2},\frac{1}{2},1\right\rangle \\ \hline \left|\frac{3}{2},1,\frac{1}{2}\right\rangle & -J & H_{AB} \\ \left|\frac{3}{2},\frac{1}{2},1\right\rangle & H_{AB} & -J \end{array}$$

$$\hat{H}_{S_T=1/2} = \begin{array}{c|cccc} |S_T,S_A,S_B\rangle & \left|\frac{1}{2},1,\frac{1}{2}\right\rangle & \left|\frac{1}{2},\frac{1}{2},1\right\rangle & \left|\frac{1}{2},0,\frac{1}{2}\right\rangle & \left|\frac{1}{2},\frac{1}{2},0\right\rangle \\ \hline \left|\frac{1}{2},1,\frac{1}{2}\right\rangle & -J & H_{AB}/2 & 0 & \sqrt{3}/2\, H_{AB} \\ \left|\frac{1}{2},\frac{1}{2},1\right\rangle & H_{AB}/2 & -J & \sqrt{3}/2\, H_{AB} & 0 \\ \left|\frac{1}{2},0,\frac{1}{2}\right\rangle & 0 & \sqrt{3}/2\, H_{AB} & J & -H_{AB}/2 \\ \left|\frac{1}{2},\frac{1}{2},0\right\rangle & \sqrt{3}/2\, H_{AB} & 0 & -H_{AB}/2 & J \end{array} \quad (7)$$

In the SDD analysis of the magnetic data, $H_{AB}$ represents a transfer integral whose magnitude reflects the degree of electronic communication and delocalization within the SQ/Cat dyad, and the exchange parameter is $J_{NN(A)\text{-}SQ(A)}$, formally the same as in the HDvV analysis (Figure 8). In order to minimize the fit parameters in this SDD model, we fixed the value of

(27) Nelsen, S. F. *Chem.—Eur. J.* **2000**, *6*, 581–588.
(28) Dinolfo, P. H.; Lee, S. J.; Coropceanu, V.; Bredas, J.-L.; Hupp, J. T. *Inorg. Chem.* **2005**, *44*, 5789–5797.
(29) Demadis, K. D.; Hartshorn, C. M.; Meyer, T. J. *Chem. Rev.* **2001**, *101*, 2655–2686.
(30) Lide, D. L., Ed. *CRC Handbook of Chemistry and Physics*, 88th ed.; CRC Press/Taylor & Francis Group: Boca Raton, FL, 2008.
(31) Kahn, O. *Molecular Magnetism*; VCH: New York, 1993.
(32) Bersuker, I. B.; Borshch, S. A. *Adv. Chem. Phys.* **1992**, *81*, 703–782.
(33) Glaser, T.; Kesting, F.; Beissel, T.; Bill, E.; Weyhermuller, T.; Meyer-Klaucke, W.; Wieghardt, K. *Inorg. Chem.* **1999**, *38*, 722–732.
(34) Blondin, G.; Girerd, J. J. *Chem. Rev.* **1990**, *90*, 1359–1376.
(35) Papaefthymiou, V.; Girerd, J. J.; Moura, I.; Moura, J. J. G.; Munck, E. *J. Am. Chem. Soc.* **1987**, *109*, 4703–4710.
(36) Girerd, J. J. *J. Chem. Phys.* **1983**, *79*, 1766–1775.

***Table 3.*** Spin Hamiltonian Fit Parameters for Complex **2**

| HDvV model | spin-dependent delocalization model | |
|---|---|---|
| | from fit to $\chi_{para}T$ | from $\Psi_u \rightarrow \Psi_g$ electronic absorption band [a] |
| $J_{NN(A)\text{-}SQ(A)} = 234\ cm^{-1}$ | $J_{NN(A)\text{-}SQ(A)} = 580\ cm^{-1}$ | $\Delta E_{Q-D} = 193\ cm^{-1}$ [b] |
| $\Delta E_{Q-D} = 234\ cm^{-1}$ [b] | $\Delta E_{Q-D} = 229\ cm^{-1}$ [b] | |
| $J_{NN(B)\text{-}SQ(A)} = 234\ cm^{-1}$ | $H_{AB} = 1750\ cm^{-1}$ (fixed) | $H_{AB} = 1750\ cm^{-1}$ |
| $\theta = -2.06$ K | $g = 1.99$ | – |
| | $\theta = -2.06$ K | – |

[a] Using $J = 234\ cm^{-1}$ from the three-state HDvV model and $\Psi_u \rightarrow \Psi_g$ band at $3500\ cm^{-1}$ gives $H_{AB} = 1750\ cm^{-1}$. [b] Quartet−doublet energy gap.

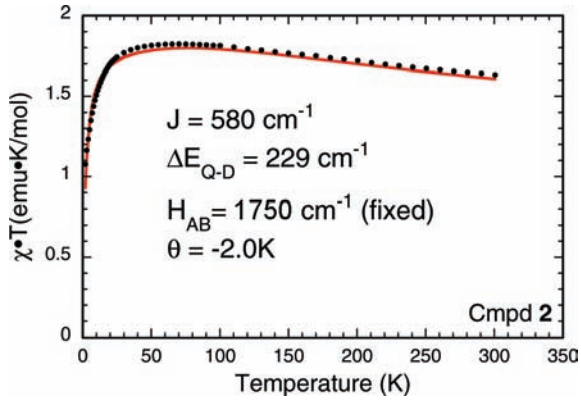


***Figure 11.*** Paramagnetic susceptibility ($\chi_{para}$) of **2** plotted as $\chi_{para}T$ vs $T$. The red line represents the best fit of the data to the SDD model described in the text.

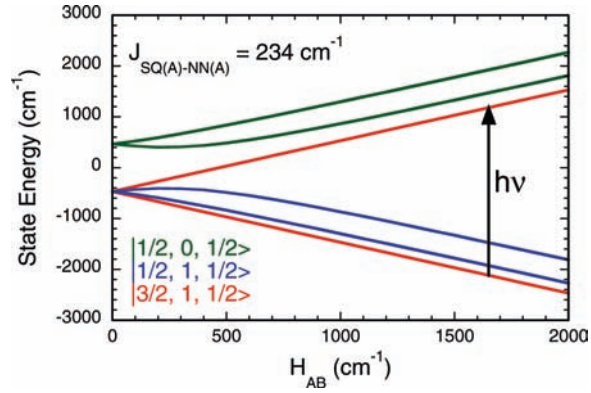


***Figure 12.*** Energy level spectrum for **2** incorporating spin-dependent delocalization. The spin basis functions are color coded. Red: $|S_T = {}^3/_2, S_A = 1, S_B = {}^1/_2\rangle$. Blue: $|S_T = {}^1/_2, S_A = 1, S_B = {}^1/_2\rangle$. Green: $|S_T = {}^1/_2, S_A = 0, S_B = {}^1/_2\rangle$. The electronic transition observed in the IR region of the spectrum is a spin allowed, bonding to antibonding $\Psi_u \rightarrow \Psi_g$ transition between $|S_T = {}^3/_2, S_A = 1, S_B = {}^1/_2\rangle$ levels split by resonance. The energy of this IR transition yields $H_{AB} \approx 1750\ cm^{-1}$ for **2**.

$H_{AB}$ to the spectroscopic value of $1750\ cm^{-1}$ determined from electronic absorption spectroscopy, and set $J_{NN(B)\text{-}SQ(A)} = 0$ due to the long superexchange pathway between SQ(A) and NN(B).[37] Thus, a high-spin ground state can only result from a nonzero $H_{AB}$. As a result, the only parameters used in fitting the magnetic data of **2** are $J_{NN(A)\text{-}SQ(A)}$, the electronic $g$-value, and an intermolecular interaction ($\theta$). The best fit of the SDD model to the data is presented in Figure 11, and the best fit parameters are $J_{NN(A)\text{-}SQ(A)} = 580\ cm^{-1}$, $g = 2$, and $\theta = -2.06$ K (Table 3). This affords an energy gap between the ground-state quartet ($Q_A$) the first doublet ($D_A$) of $229\ cm^{-1}$.

The resultant energy level spectrum (Figure 12) that derives from eq 7 requires some comment, as it differs substantially from that commonly encountered for transition metal systems that have been observed to display spin-dependent delocalization.[32,38] This difference is due to the comparatively weak "single-site" exchange resulting from the 1,4-phenylene bridge[39] and parametrized by the magnitude of $J_{NN(A)\text{-}SQ(A)}$. Coupled with the magnitude of $H_{AB}$, this leads to a strong configurational mixing between the $|S_T = {}^1/_2, S_A = 1, S_B = {}^1/_2\rangle$ and $|S_T = {}^1/_2, S_A = 0, S_B = {}^1/_2\rangle$ states, and this wave function mixing is clearly evident in Figure 12. In marked contrast to transition metal systems, the "single-site" exchange term in **2** is significantly reduced by 2−3 orders of magnitude. Thus, for transition metal systems there is negligible mixing between energy levels with the same $S_T$ that derive from different electronic configurations and are therefore

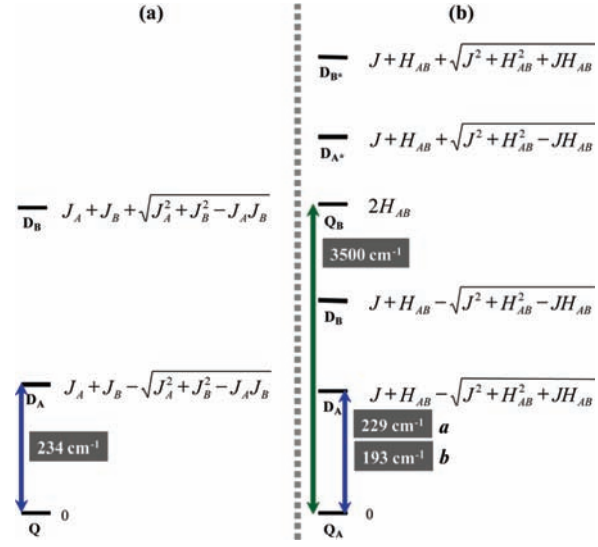


***Figure 13.*** Energy level diagrams for spin states derived in the text using different spin Hamiltonian models for **2**. (a) Three state/two $J$ HDvV model; $J_A = J_{NN(A)\text{-}SQ(A)}$; $J_B = J_{NN(B)\text{-}SQ(A)}$. (b) SDD model with $J = J_{NN(A)\text{-}SQ(A)}$. [a]Quartet−doublet gap from SDD fit of $\chi_{para}T$. [b]Quartet−doublet gap from $\Psi_u \rightarrow \Psi_g$ electronic absorption band, see text.

completely ignored in the analysis of transition metal systems that display spin-dependent delocalization phenomena. The incorporation of the $|S_T = {}^1/_2, S_A = 0, S_B = {}^1/_2\rangle$ "non-Hund"[32] states is extremely important in the development of a proper description of both the ground- and excited-state properties of these organic mixed-valence systems that possess high-spin ground states resulting from spin-dependent electron delocal-

(37) Theory shows that for $H_{AB} > \sim 1000\ cm^{-1}$ the lowest quartet−doublet energy gap is essentially invariant to further increases in $H_{AB}$. This results in $H_{AB}$ being insensitive to the energy gap (see Figure 12), and necessitates an *a priori* estimate of $H_{AB}$ from optical data (see Supporting Information).

(38) Gamelin, D. R.; Bominaar, E. L.; Kirk, M. L.; Wieghardt, K.; Solomon, E. I. *J. Am. Chem. Soc.* **1996**, *118*, 8085–8097.

(39) Shultz, D. A.; Fico, R. M., Jr.; Bodnar, S. H.; Kumar, R. K.; Vostrikova, K. E.; Kampf, J. W.; Boyle, P. D. *J. Am. Chem. Soc.* **2003**, *125*, 11761–11771.

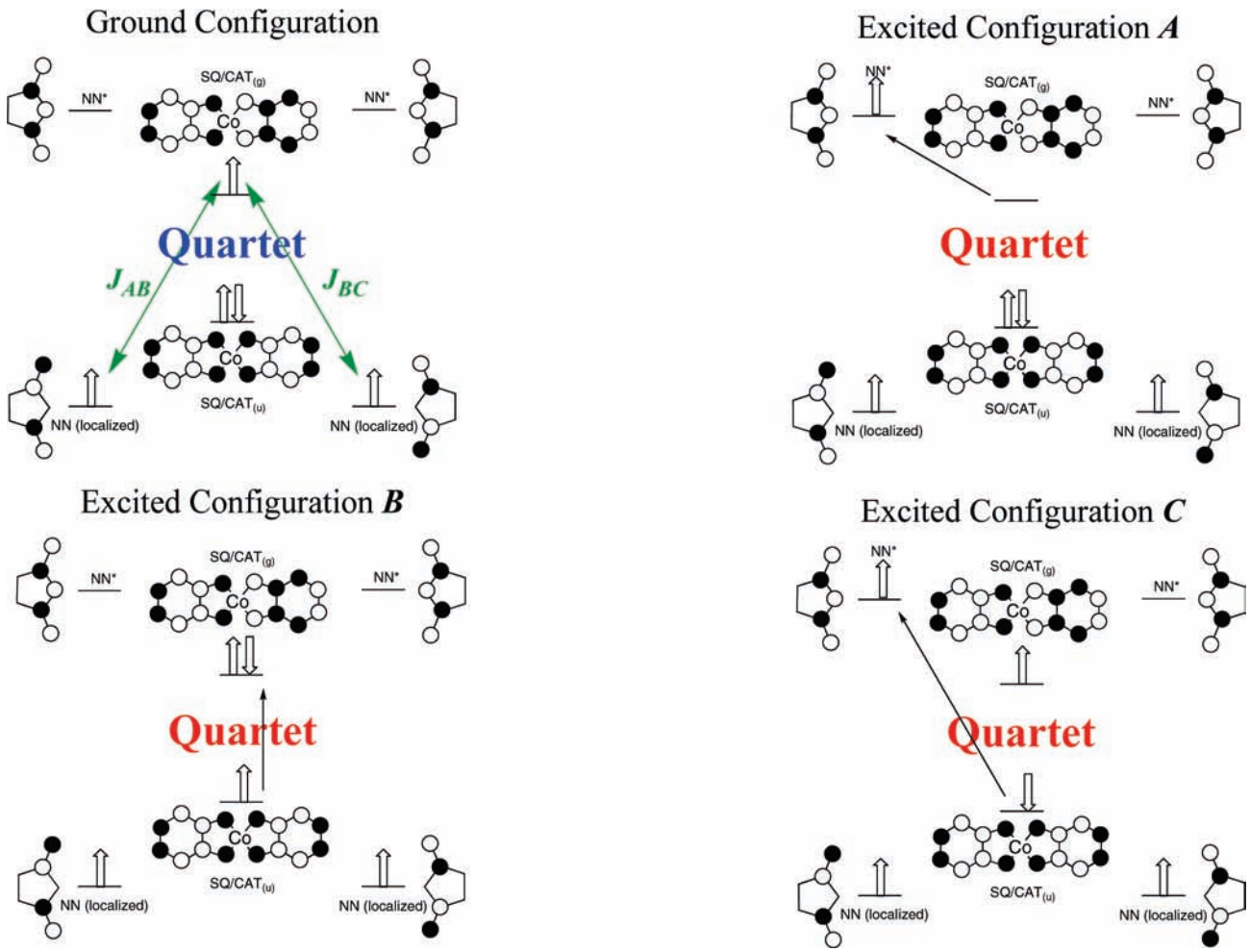


***Figure 14.*** Energy diagram depicting the relationship between HDvV exchange parameters ($J_{AB}$ and $J_{BC}$) and the $Co^{III}(dioxolene)_2$ (donor) → NN (acceptor) charge transfer configurations that result from a delocalized $Co^{III}(diox)_2$ one-electron promotion to the NN* orbitals.

ization. The resulting energy levels obtained from the antisymmetric HDvV and SDD analyses are summarized in Figure 13.

## Discussion

We have attempted to assess the degree of electronic delocalization in both **1** and **2** by X-ray crystallography, optical spectroscopy, analyses of the magnetic susceptibility data, bonding calculations, and spin density distributions. The observation of (1) a low-energy absorption feature in the IR−NIR region of the spectrum demonstrating a slight solvent dependence, (2) sharp deviations in bandwidth from the Hush prediction, (3) a $J_{NN(B)\text{-}SQ(A)}/J_{NN(A)\text{-}SQ(A)}$ ratio of unity determined from the HDvV analysis, and (4) calculated ground-state structures and spin density distributions, all point toward a high degree of delocalization and a Class II/III to Class III electronic description for the Cat/SQ dyads in **1** and **2**.[29] Provided **1** and **2** reside in the Class II/III limit, the dominant contribution to electronic localization and a barrier to thermal electron transfer most likely results from an in-plane distortion of $b_u$ symmetry due to vibronic coupling between the low-lying $^4B_g$ excited state and the $^4A_u$ ground state. Unfortunately, the crystallographic data do not allow for a direct determination of this structural distortion due to the presence of a crystallographically imposed inversion center at the Co ion. In light of the planar $Co(diox)_2$ cores, it is of interest to note that mixed-valent *o*-dimethyltetrathiafulvalene cation radical dimers that possess either dimethylsilicon or dimethylgermanium bridges display planar geometries and isotropic proton hyperfine coupling constants consistent with Class III behavior and complete delocalization of the radical electron over the entire molecule on the EPR timescale.[40] The calculated HOMO and SOMO for the *o*-dimethyltetrathiafulvalene cation radical dimers are remarkably similar those of **1** and **2** and possess $a_u$ and $b_g$ symmetry, respectively.[40] Despite a very low HOMO−LUMO gap (~500 $cm^{-1}$) calculated for the neutral species, the data do not provide any evidence for localization due to the presence of an in-plane $b_u$ distorting vibration resulting from vibronic coupling.[40]

It is of interest to understand how electron delocalization could be mediated by a low-spin *diamagnetic* Co(III) center that bridges the two dioxolene units in **1** and **2**. In the high delocalization limit (i.e., a low thermal barrier for electron transfer) effective $C_{2h}$ symmetry is appropriate in the analysis of the data. Here, the local symmetry of the doubly occupied $\Psi_u$ orbital lacks the appropriate symmetry to mix with any of the Co d-orbitals, as the latter possess *gerade* symmetry. However, the $\Psi_g$ dioxolene orbital does possess the correct symmetry to mix with the Co $d_{xz}$ orbital to provide a metal-assisted pathway promoting electron delocalization of the $\Psi_g$ electron. Thus, an effective electron delocalization is primarily

(40) Biaso, F.; Geoffroy, M.; Canadell, E.; Auban-Senzier, P.; Levillain, E.; Fourmigue, M.; Avarvari, N. *Chem.—Eur. J.* **2007**, *13*, 5394–5400.

facilitated by p−d−p $\pi$-overlap ($H_{AB} \approx 1750$ cm$^{-1}$) between p-orbitals on different dioxolene ligands bridged by the Co $d_{xz}$ orbital.

We can now describe how localized NN spins separated by 22 Å can be coupled via valence delocalization within the SQ/Cat dyad, and relate this mechanism to that proposed for high $T_c$ ferromagnetism in DMSs. Schematic energy level diagrams that describe this mechanism within a valence-bond configuration interaction framework are presented in Figure 14. It is important to note that the $J_{AB}$ and $J_{BC}$ exchange interactions which couple NN(A) and NN(B) via the delocalized itinerant electron do not derive from direct NN-(SQ/Cat) wave function overlap. This is because the localized NN SOMOs are orthogonal to the singly occupied $\Psi_g$. Thus, the coupling of these localized NN moments occurs via two excited-state charge transfer configurations (***A*** and ***C***, Figure 14). Excited configurations ***A*** and ***C*** result from (SQ/Cat) → NN* donor−acceptor charge transfer and contribute directly to the stabilization of the $S_T = {}^3/_2$ ground state via configurational mixing. Within this VBCI model, excited-state configuration ***B*** represents an excitation within the SQ/Cat dyad and does not couple the localized NN moments. The contributions of excited-state configurations ***A*** and ***C*** to the $S_T = {}^3/_2$ ground state follow the same paradigm we previously used to explain the electronic origin of strong ferromagnetic exchange within individual SQ-NN donor−acceptor biradical ligands.[41,42] Mixing of these excited configurations into the ground-state wave function is the mechanism by which covalency is introduced into the NN*-(SQ/Cat) bonding scheme to form delocalized $\Psi_u$ and $\Psi_g$ wave functions. This admixture of NN* character into the delocalized (SQ/Cat) wave function is clearly evident upon inspection of the delocalized $\Psi_u$ and $\Psi_g$ wave functions in Figure 5. When coupled to a strong ferromagnetic single-site NN*-NN exchange ($2K \approx 4000$ cm$^{-1}$),[42] this results in ferromagnetic coupling of localized moments over nanoscale distances. Thus, an itinerant electron can couple to a donor−acceptor-type charge transfer state to yield very long coherence lengths for the itinerant electron, and this itinerant electron can interact via a strong single-site exchange integral ($K$) to promote long-range ferromagnetic exchange coupling in molecular systems, and ferromagnetism in materials of higher dimensionality.

(41) Kirk, M. L.; Shultz, D. A.; Depperman, E. C. *Polyhedron* **2005**, *24*, 2880.
(42) Kirk, M. L.; Depperman, E. C.; Shultz, D. A.; Brannen, C. L. *J. Am. Chem. Soc.* **2007**, *129*, 1937–1943.

## Conclusions

Compounds **1** and **2** are prototypes of strong spin-dependent delocalization and ferromagnetic exchange using purely organic spin-bearing units. It is of fundamental importance that the high-spin nature of **1** and **2** are only made possible via SQ/Cat valence delocalization in the Class II/III to Class III limit with the excess electron being coupled to excited state donor−acceptor charge transfer configurations that involve virtual orbitals on the NN fragments. In this respect, the strong interaction between a delocalized electron and the "localized" NN moments resembles the exchange interaction between delocalized electrons and pinned magnetic impurities in magnetically doped semiconductors leading to the observed ferromagnetism in these materials. We also suggest that modeling magnetic susceptibility of mixed-valent systems having localized radicals covalently attached to each partner of a mixed-valent dyad may provide an excellent handle for evaluating delocalization. Furthermore, we have shown that valence delocalization mediated by the organic $\pi$-system can lead to very long-range electron correlation (>22 Å) that is difficult to obtain in classic molecular mixed-valence transition metal systems.

**Acknowledgment.** M.L.K. acknowledges the National Institutes of Health (GM-057378) and the National Science Foundation (NSF CHE-0616190) for financial assistance. D.A.S. thanks the National Science Foundation (CHE-0345263/0910585) for financial support, and the Camille and Henry Dreyfus Foundation for a Camille Dreyfus Teacher-Scholar Award. H.L. acknowledges the Creative Research Initiatives Program Research Fund (Project title: Smart Molecular Memory) of MEST/KOSEF. We acknowledge Dr. Paul D. Boyle of North Carolina State University and Dr. Jeff Kampf of the University of Michigan for X-ray crystallographic data collection and refinement, and we thank Dr. Peter S. White and the Department of Chemistry at the University of North Carolina at Chapel Hill for use of their Apex2 diffractometer.

**Supporting Information Available:** Crystallographic details, CIF files, saturation magnetization plots, electronic absorption spectra and supporting magnetic susceptibility plots, and complete ref 12. This material is available free of charge via the Internet at http://pubs.acs.org.

JA904648R